

1 **BrGDGTs-based seasonal paleotemperature reconstruction for the last 15,000 years**
2 **from a shallow lake on the eastern Tibetan Plateau**

3 Xiaohuan Hou ^a, Nannan Wang ^a, Zhe Sun ^b, Kan Yuan ^{a,c}, Xianyong Cao ^a, Juzhi Hou ^{a*}

4 ^a *Group of Alpine Paleocology and Human Adaptation (ALPHA), State Key Laboratory of Tibetan*
5 *Plateau Earth System, Resources and Environment (TPESRE), Institute of Tibetan Plateau Research,*
6 *Chinese Academy of Sciences, Beijing 100101, China*

7 ^b *Institute of Geography and Resources Science, Sichuan Normal University, Chengdu, 610066, China*

8 ^c *University of Chinese Academy of Sciences, Beijing 100049, China*

9

10 * Corresponding author

11 E-mail address: houjz@itpcas.ac.cn

12

13 **ABSTRACT**

14 Knowledge of Holocene temperature changes is crucial for addressing the problem of the
15 discrepancy between Holocene proxy temperature reconstructions and climate model
16 simulations. The complex spatiotemporal pattern of temperature variations on the Tibetan
17 Plateau (TP) further complicates the study of Holocene continental climate change. The
18 discrepancy between model-based and proxy-based Holocene temperature reconstructions
19 possibly results from the seasonal biases and environmental ambiguities of the proxies.
20 Quantitative temperature reconstructions using different proxies from the same sediment core
21 can provide an effective means of evaluating different proxies; however, this approach is
22 unusual in terrestrial environments. Here, we present an ice-free-season temperature record
23 for the past 15 ka from a shallow, freshwater lake on the eastern TP, based on brGDGTs
24 (branched glycerol dialkyl glycerol tetraethers). This record shows that the Holocene Thermal
25 Maximum lags the pollen-based July temperature recorded in the same sediment core. We
26 conclude that the mismatch between the brGDGTs-based and pollen-based temperatures is
27 primarily the result of seasonal variations in solar irradiance. The overall pattern of
28 temperature changes is supported by other summer temperature records, and the Younger
29 Dryas cold event and the Bølling–Allerød warm period are also detected. A generally warm
30 period occurred during 8–3.5 ka, followed cooling in the late Holocene. Our findings have
31 implications for understanding the seasonal signal of brGDGTs in shallow lakes, and provide
32 critical data for confirming the occurrence of seasonal biases in different proxies from high-
33 elevation lakes. To further investigate the significance of the brGDGTs and temperature
34 patterns on the TP, we reviewed previously published brGDGTs-based Holocene temperature

35 records across the TP. ~~The results demonstrate that brGDGTs have been employed to~~
36 ~~reconstruct various temperatures in different studies, including annual average temperature~~
37 ~~and warm-biased temperature, and that both show a gradual warming trend~~ In these studies,
38 brGDGTs have been interpreted to reflect either mean annual air temperature or growing
39 season temperature. In both cases, brGDGTs reflect a gradual warming trend during the
40 Holocene with relatively cooler conditions during the middle Holocene, and a cooling trend
41 during the middle to late Holocene. We analyzed the possible reasons for the diverse
42 brGDGTs records on the TP and emphasize the importance of considering lake conditions
43 and modern investigations of brGDGTs in lacustrine systems when using brGDGTs to
44 reconstruct paleoenvironmental conditions.

45 **Keywords:** Tibetan Plateau, brGDGTs, the mean temperature of Months Above Freezing,
46 shallow lake, Holocene

47 **1 Introduction**

48 Global climate change has had a profound impact on both the natural ecological and socio-
49 economic systems that are vital for human survival and development, making climate change
50 a critical limiting factor for the sustainable development of human society. The Tibetan
51 Plateau (TP), also called the “Third Pole” (Qiu, 2008), has undergone a more rapid warming
52 over the last five decades, with a rate twice that of the global average (0.3 – 0.4°C/decade)
53 (Kuang and Jiao, 2016; Chen et al., 2015), making it one of the world's most temperature-
54 sensitive regions (Chen et al., 2015; Yao et al., 2022). Consequently, assessing the impact of
55 future climate change on the TP is becoming increasingly important. To enhance the
56 precision and accuracy of future climate change estimates for the TP under ongoing global

57 climate change and to minimize the uncertainty in climate simulations, it is essential to
58 investigate the processes and mechanisms of regional climate and environmental changes,
59 with particular emphasis on temperature, on a relatively long timescale, such as that of the
60 Holocene.

61
62 The Holocene, the most recent geological epoch, is closely linked with the development of
63 human civilization. Quantitative reconstructions of Holocene temperature trends can be used
64 to explore their impacts on civilization and to establish a geological and historical context for
65 predicting future climate changes. In recent decades, many Holocene quantitative
66 reconstructions of seasonal and annual temperatures for the TP have been produced using
67 various proxies, like pollen (Herzschuh et al., 2014; Lu et al., 2011), chironomids (Zhang et
68 al., 2017; Zhang et al., 2019a), $\delta^{18}\text{O}$ in ice cores (Pang et al., 2020; Thompson et al., 1997),
69 and biomarkers (Hou et al., 2016; Zhao et al., 2013; Cheung et al., 2017). These
70 reconstructions have provided crucial data for the elucidation of Holocene temperature
71 changes. However, the available Holocene temperature records from the TP show divergent
72 trends. Multiple proxy indicators indicate three different Holocene temperature patterns on
73 the TP. First, a consistent Holocene warming trend (Sun et al., 2022; Feng et al., 2022; Opitz
74 et al., 2015). For example, brGDGTs based annual temperatures (Feng et al., 2022; Sun et al.,
75 2022) indicate a gradual warming trend which resembles the $\delta^{18}\text{O}$ temperature record from
76 the Chongce ice core on the western TP, except for the last 2 ka (Pang et al., 2020). Second,
77 an early to middle Holocene summer temperature maximum and a gradual cooling trend
78 during the late Holocene are observed in pollen-, alkenone- and chironomid-based
79 temperature records (Herzschuh et al., 2014; Hou et al., 2016; Zhang et al., 2017; Wang et al.,

80 [2021a](#); [Zheng et al., 2015](#)). Third, a prominent relatively cool middle Holocene ([Wang et al.,](#)
81 [2021c](#); [Li et al., 2017](#)); for example, a composite temperature record suggests that
82 temperatures were ~2°C cooler during the middle Holocene than during the early and late
83 Holocene ([Wang et al., 2021c](#)). Several records also show a steady long-term trend without
84 distinct cooling or warming ([Sun et al., 2021](#)). Moreover, the cooling trends in proxy-based
85 Holocene temperature records are inconsistent with those of climate models, which indicate a
86 warming trend, and this inconsistency is widely known as the “Holocene temperature
87 conundrum” ([Liu et al., 2014](#)). There are several potential factors that may contribute to the
88 disparity in Holocene temperature trends, including seasonal biases and uncertainties in
89 temperature proxies and reconstructions, independent of climate models ([Liu et al., 2014](#);
90 [Hou et al., 2019](#); [Bova et al., 2021](#); [Cartapanis et al., 2022](#); [Marsicek et al., 2018](#)). While
91 several recent studies have suggested that seasonality in proxies is not the major cause of the
92 Holocene temperature conundrum ([Dong et al., 2022](#); [Zhang et al., 2022b](#)), it is significant
93 that the TP is an alpine and high-altitude region with significant seasonal temperature
94 variations. Moreover, most organisms tend to grow during the warmer seasons at high
95 latitudes and high altitudes ([Zhao et al., 2021a](#)). Currently, however, we lack unambiguous
96 and reliable seasonal temperature records to support a seasonality-bias hypothesis. Extensive
97 research has been conducted in lakes, employing a single proxy to reconstruct past
98 temperature fluctuations. However, there have been scarce studies that employ various
99 proxies within the same core to reconstruct paleotemperature variations. Furthermore, the
100 limited number of studies primarily concentrate on reconstructing summer temperature and
101 annual average temperature. For example, a chironomid-based July temperature

102 reconstruction for Tiancai lake on the southeastern TP shows higher temperatures during the
103 early to middle Holocene (Zhang et al., 2017), while the brGDGTs-based annual average
104 temperature shows a warming trend (Feng et al., 2022). Different proxies may reflect the
105 seasonal temperatures in different months, and thus producing temperature reconstructions
106 for different months for the same sediment core may help better understand the seasonal bias
107 of terrestrial temperature records. Furthermore, the reconciliation of the divergent trends of
108 Holocene temperature on the TP and its surroundings requires additional high-altitude
109 temperature records from these regions, with reliable chronologies and proxy records with an
110 unambiguous climatological significance.

111
112 Branched glycerol dialkyl glycerol tetraethers (brGDGTs) are a group of membrane-spanning
113 lipids found in bacteria (Fig. S1) (Chen et al., 2022; Halamka et al., 2022; Sinninghe Damsté
114 et al., 2000), and they have become a powerful tool for quantifying past terrestrial
115 temperature variations. Through investigations of brGDGTs in globally-distributed soils, it
116 was found that the distribution of brGDGTs is primarily related to temperature and pH
117 (Weijers et al., 2007). Subsequently, brGDGTs–temperature calibrations from soil, peat and
118 lake sediments were established on scales from global (Weijers et al., 2007; De Jonge et al.,
119 2014; Crampton-Flood et al., 2020; Martínez-Sosa et al., 2021) to regional (e.g., East Asia)
120 (Sun et al., 2011; Ding et al., 2015; Wang et al., 2016; Dang et al., 2018), leading to
121 considerable progress in reconstructing terrestrial temperatures, particularly on the TP
122 (Cheung et al., 2017; Zhang et al., 2022a; Li et al., 2017).

123

124 Natural lakes are widely distributed across the TP (Zhang et al., 2019b). Lake sediments,
125 characterized by their organic matter-rich composition, exhibit continuous and rapid
126 accumulation rates. As a result, they offer high-resolution records of environmental changes,
127 making them highly valued as a primary terrestrial climate archive (Moser et al., 2019).
128 BrGDGTs in lacustrine systems are often more strongly correlated with temperature, with
129 higher coefficient of determination (r^2) and lower root mean square error (RMSE) values
130 (Martínez-Sosa et al., 2021), than in soils and peats. ~~However~~Nevertheless, the factors that
131 impact the distribution of brGDGTs in lakes are intricate and multidimensional. Notably, the
132 sources of brGDGTs within lakes are intricate, involving contributions from soil as well as
133 autochthonous lake processes. ~~Moreover~~However, an expanding body of research
134 underscores a substantial prevalence of autochthonous brGDGTs in lakes (Tierney and
135 Russell, 2009; Tierney et al., 2010; Weber et al., 2015; Wang et al., 2021b). Furthermore, the
136 origins of brGDGT producers remain uncertain and could be influenced by various factors,
137 including lake salinity (Wang et al., 2021b), redox conditions (Weber et al., 2018), oxygen
138 content and/or mixing patterns (Van Bree et al., 2020; Wu et al., 2021; Buckles et al., 2014).
139 Additionally, even lake depth plays a role due to distinct ecological niches (Woltering et al.,
140 2012), thereby contributing to the intricate interplay that shapes the distribution of brGDGTs
141 within lakes.

142
143 In this study, we obtained a quantitative temperature reconstruction for the past 15 ka from
144 Gahai, a shallow (average depth of ~2 m) freshwater lake located in the source area of the
145 Yellow River. This region is an important ecological protection area on the eastern edge of

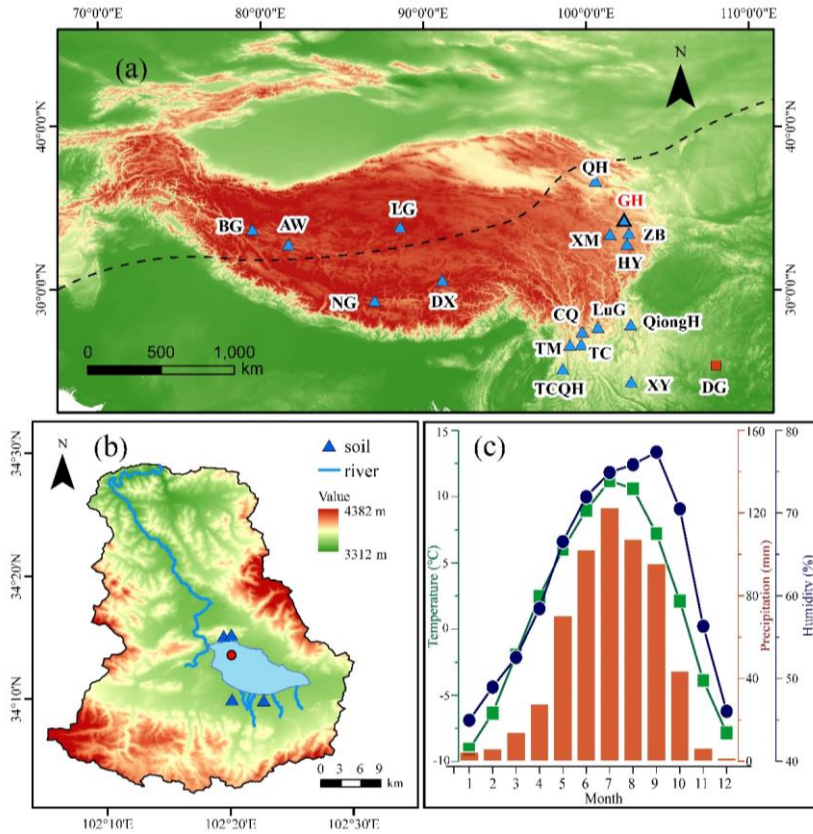
146 the TP. Freshwater environments avoid the confounding effects of salinity on brGDGTs-
147 based temperature reconstructions, and shallow lakes also minimize the impact of the uneven
148 distribution of light and nutrients on brGDGTs. Our specific aims were: (1) to determine the
149 long-term trend of Holocene warm-biased terrestrial temperatures at a high elevation; (2) to
150 compare records of ice-free season temperatures with July temperatures from the same
151 sediment core; and (3) to gain a better understanding of the possible mechanisms responsible
152 for Holocene temperature variations, especially on the TP.

153 **2 Materials and methods**

154 *2.1 Study site*

155 Gahai (102°11'–102°28' E, 34°04'–34°4' N, 3444 m a.s.l.) is a freshwater lake and part of the
156 Gahai meadow wetland, which is a national nature reserve with restricted human access, on
157 the eastern edge of the Tibetan Plateau (Fig. 1). The lake is fed by runoff from the
158 surrounding hills, drains into the Tao River, and ultimately enters the Yellow River. Thus,
159 Gahai lake is a critical water conservation area in the upper reaches of the Yellow River. The
160 average water depth of Gahai is ~1–2 m, and the maximum depth is ~5 m. The vegetation in
161 the catchment consists mainly of *Kobresia tibetica*, *Equisetum arvense*, *Potentilla anserina*,
162 *Artemisia subulate*, and *Oxytropis falcata* (Ma et al., 2019). Meteorological data for the area
163 are available from Langmu Temple station (1957-1988) (Fig. 1) (102°38' E, 34°5' N, 3412 m
164 a.s.l.), ~32 km northwest of Gahai lake. They indicate an annual average (mean) precipitation
165 of 781 mm, with > 67% occurring between June and September, and mean annual
166 temperature of 1.2 °C with a relative humidity of ~65%. The summers are mild and humid
167 and the winters are cold and dry. From May to September, the mean average temperature is

168 above freezing (0°C), but the temperature in May is very low, close to 0°C .



169
 170 **Fig. 1** (a) Locations of the sites on the Tibetan Plateau referenced in the text. Triangle with
 171 bold line indicates the location of Gahai lake (this study). Other triangles indicate the
 172 locations of cited studies on the Tibetan Plateau and the surrounding area: Bangong Co
 173 (BG), Aweng Co (AW), Ngamring Co (NG), Linggo Co (LG), Dangxiong wetland (DX),
 174 Qinghai lake (QH), Ximen Co (XM), Zoige Basin (ZB), Hongyuan peatland (HY), Lugu
 175 lake (LuG), Cuoqia lake (CQ), Tingming lake (TM), Tengchongqinghai lake (TCQH),
 176 Tiancai lake (TC), Qionghai lake (QH), Xingyun lake (XY). Red square indicates
 177 Dongge Cave (DG). Black dotted line represents the northern boundary of the modern
 178 Asian summer Monsoon (Chen et al., 2008). (b) Drainage basin of Gahai lake and the

179 core site. (c) Climate data from Langmu Temple meteorological station: monthly
180 temperature (green line), precipitation (red bars), and humidity (blue line).

181 2.2 Sampling

182 A sediment core with the length of 329 cm was obtained from Gahai Lake in January 2019, at
183 a water depth of 1.95 m, using a UWITEC platform operated from the frozen lake surface. In
184 addition, four catchment soil samples were collected from around the lake (Fig. 1). All
185 samples were transported to the Institute of Tibetan Plateau Research, Chinese Academy of
186 Sciences (ITPCAS). The sediment core was split lengthwise, and one half was subsampled
187 and freeze-dried for subsequent analysis.

188

189 2.3 Chronology

190 The chronology of the upper 20 cm of the sediment core is based on measurements of ^{210}Pb
191 and ^{137}Cs , at a 1-cm interval. The chronology for the deeper part of the core is provided by
192 accelerator mass spectrometry (AMS) ^{14}C measurements of 13 bulk sediment samples, which
193 were conducted by Beta Analytic Inc. (Miami, USA) (Fig. 2) (Wang et al., 2022).

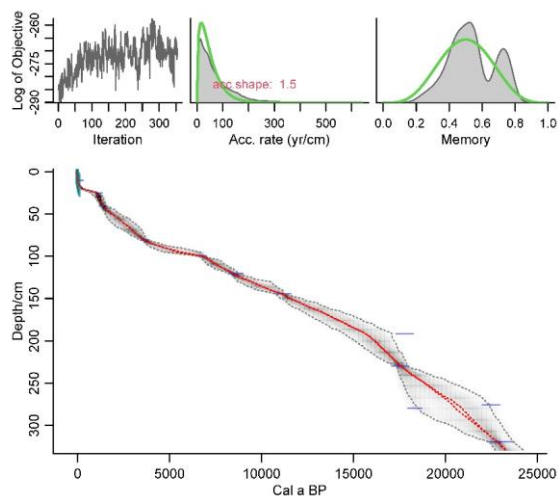
194

195 The ^{210}Pb age model was constructed using the constant rate of supply (CRS) model and the
196 ^{137}Cs peak was used as supplement (Appleby, 2002). The calculated age of ^{210}Pb using CRS
197 model aligned well with the ^{137}Cs peak at 6 cm. Overall, the CRS model was deemed suitable
198 for determining the age of Gahai lake.

199

200 Reservoir age, as highlighted by Hou et al. (2012), is a crucial factor affecting the age
201 determination of lake sediment cores on the TP. Therefore, it was necessary to establish the

202 reservoir age of Gahai lake before undertaking paleoclimate reconstruction. The linear
203 extrapolation relationship between the ^{14}C ages and depth to the sediment-water interface is
204 often used to estimate the reservoir age. The ^{14}C age of 13 samples exhibits a good linear
205 relationship with sediments depth in Gahai lake. Extrapolation of this 13 ^{14}C ages down to the
206 depth of 6 cm yielded a ^{14}C age of 461 yr BP, while the reliable ^{210}Pb age at 6 cm is -27 yr BP.
207 Consequently, the difference between the two ages, which amounts to 488 yr, was taken as
208 the reservoir age. Additionally, it's worth noting that independent estimations of the ^{14}C
209 calibration age and ^{210}Pb age around 10 cm in Gahai lake was obtained, resulting in values of
210 497 yr BP and 18 yr BP, respectively. The difference of 479 yr between these two ages can
211 also be considered as the reservoir age. These two methods of estimating reservoir age of
212 Gahai lake show very close, which are mutually supportive. So, the average of 483 yr was
213 adopted as the reservoir age. All original ^{14}C dates were corrected by subtracting the reservoir
214 age (483 yr) and calibrating them to calendar ages using Calib 8.1. The age-depth model (Fig.
215 2) was constructed using the Bacon program with the ^{14}C ages and ^{210}Pb ages (Blaauw and
216 Andres Christen, 2011) and was reported by Wang et al. (2022).



217
 218 **Fig. 2** Age-depth model for Gahai, based on AMS ^{14}C , ^{210}Pb and ^{137}Cs ages (Wang et al.,
 219 2022). The ages of the upper 20 cm are based on ^{210}Pb and ^{137}Cs dating (green symbols)
 220 and those of the lower part on AMS ^{14}C dates (blue symbols).

221

222 2.4 Lipids extraction and brGDGTs analysis

223 For lipids extraction, ~5 g samples were ground to a powder and extracted ultrasonically with
 224 dichloromethane (DCM): methanol (MeOH) (9: 1, v: v) three times. The supernatants were
 225 combined and dried under a stream of nitrogen gas. Subsequently, the total lipid extracts were
 226 separated into neutral and acid fractions through a LC-NH₂ silica gel column using DCM:
 227 isopropyl alcohol (2: 1, v: v) and ether with 4% acetic acid (v: v), respectively. The neutral
 228 fraction was then eluted through a silica gel column using n-Hexane, DCM and MeOH, and
 229 the GDGTs were dissolved in the MeOH. The GDGTs fraction was passed through a 0.45 μm
 230 polytetrafluoroethylene (PTFE) filter before analysis. C₄₆-GDGT (a standard compound)
 231 (Huguet et al., 2006) was added to the samples before analysis.

232

233 BrGDGTs were detected using an HPLC-APCI-MS (Waters ACQUITY UPLC I-Class/Xevo
234 TQD) with auto-injection at the ITPCAS. The compounds were separated by three Hypersil
235 Gold Silica LC columns in sequence (each 100 mm × 2.1 mm, 1.9 μm, Thermo Fisher
236 Scientific; USA), maintained at a temperature of 40°C. GDGTs were eluted isocratically
237 using 84% hexane and 16% ethyl acetate (EtOA) for the first 5 min, followed by a linear
238 gradient change to 82% hexane and 18% EtOA from 5 to 65 min. The columns were cleaned
239 using 100% EtOA for 10 min, and then back to 84% hexane and 16% EtOA to equilibrate the
240 column, with a flow rate of 0.2 ml min⁻¹.

241

242 The APCI-MS conditions were as follows: nebulizer pressure at 60 psi, APCI probe
243 temperature at 400°C, drying gas flow rate of 6 L/min and temperature of 200°C, capillary
244 voltage of 3600 V, source corona of 5.5 μA. Detection was performed in selected ion
245 monitoring (SIM) mode, targeting the protonated molecules at m/z 1050, 1048, 1046, 1036,
246 1034, 1032, 1022, 1020, 1018 and 744. The results were analyzed using MassLynx V4.1
247 software, and quantification was achieved by comparing the peak areas of targeted ions and
248 the internal standard, assuming an identical response factor for GDGTs.

249

250 **3 Results and Discussion**

251 *3.1. Concentration and distribution of brGDGTs in the sediment core and catchment soils*

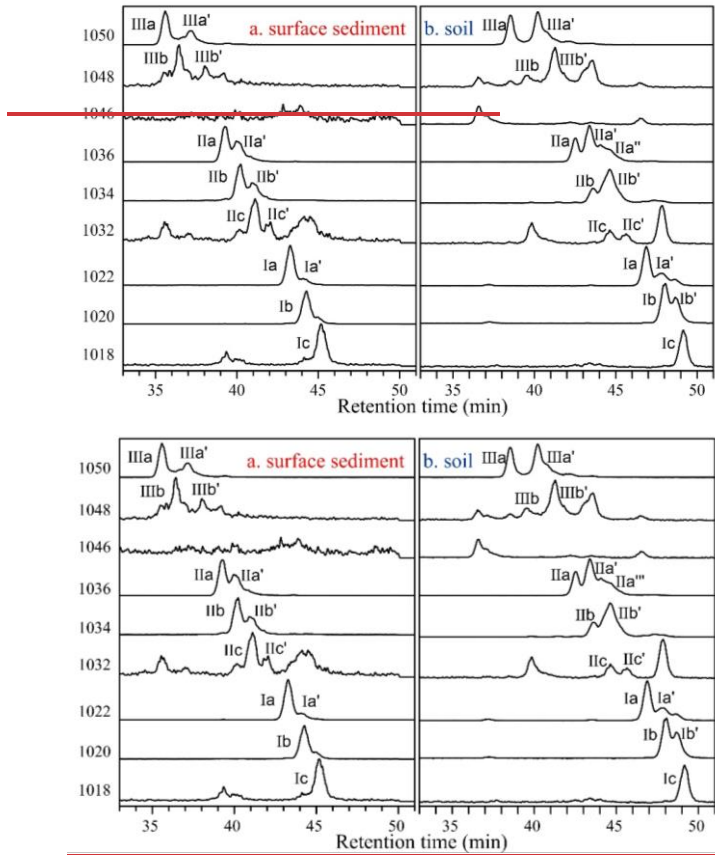
252 BrGDGTs were detected in both the catchment soils and the downcore sediments. The
253 average concentration of brGDGTs in the catchment soils (0.07 ng g⁻¹dw) was lower than in
254 the surficial core sediments (0.70 ng g⁻¹dw). In the soil samples, pentamethylated brGDGTs

255 were generally the most ~~abundance~~abundant (55.33%), followed by tetramethylated
256 brGDGTs (23.60%) and hexamethylated brGDGTs (21.07%) (Fig. S2). The relative amount
257 of cyclopentane ring-containing brGDGTs in the soil samples was generally low (24.34%)
258 and it was sometimes too low to be detected, especially the fractions of IIIb, IIIb', IIIc, IIIc',
259 IIIc and IIIc'. In the downcore sediments, the relative ~~abundance~~abundant of tetramethylated
260 brGDGTs (43.84%) was like that of pentamethylated brGDGTs (41.93%), and
261 hexamethylated brGDGTs were the least ~~abundance~~abundant (14.22%) (Fig. S2). The
262 relative abundant of cyclopentane ring-containing brGDGTs in the downcore sediments
263 (67.82%) was lower than that in the catchment soils.

264 3.2 *In situ* production of brGDGTs in Gahai lake

265 Although lacustrine brGDGTs have great potential for quantitatively reconstructing terrestrial
266 paleotemperatures, uncertainties about their sources in lacustrine environments are a major
267 factor limiting their application (Tierney and Russell, 2009; Cao et al., 2020; Sun et al., 2011;
268 [Sinninghe Damsté et al., 2009](#); [Buckles et al., 2014](#)). To investigate the origin and
269 characteristics of brGDGTs in the Gahai lake sediments, we examined the distributions and
270 concentrations of brGDGTs in the sediments and catchment soils and found notable
271 differences between them. First, as described in the previous section, the average content of
272 brGDGTs in the catchment soils was ~10% that of the surficial lake sediments, suggesting the
273 absence of large-scale allochthonous inputs from the catchment soils. Second, the brGDGTs
274 distributions in the downcore sediments were quite different from those in the catchment soils,
275 which suggests a substantial autochthonous brGDGTs contribution to the lake sediments (Fig.
276 3 and Fig. S2). Moreover, the ratios of 6-methyl brGDGTs to 5-methyl GDGTs (IR_{6ME}) in the

277 soils and sediments, calculated according to the formula proposed by [De Jonge et al. \(2014\)](#),
278 were different. In the soil samples, IR_{6ME} varied between 0.54 and 0.57 and the average ratio
279 in the downcore samples was 0.26, varying between 0.18 and 0.47. Third, the in-situ
280 production of brGDGTs in Gahai lake is suggested by the discrepancies in the degree of
281 methylation (MBT'_{5ME}) between the soils and surface sediments. The average value of
282 MBT'_{5ME} in the Gahai lake surface sediments was 0.48, which is clearly higher than in the
283 catchment soils, with the range of 0.32–0.35. Fourth, and potentially the most significant, the
284 IIIb' and Ib' compounds are present in the catchments soil but not in the Gahai lake surficial
285 sediments, which may be direct evidence of an autochthonous brGDGTs contribution in the
286 lacustrine environment (Fig. 3), and a lower proportion of soil-derived brGDGTs input.
287 Therefore, we conclude that the brGDGTs in the Gahai lake sediments are mainly of in-situ
288 origin.



289

290

291 **Fig. 3** Representative high-performance liquid chromatography/atmospheric pressure
 292 chemical ionization-mass spectrometry (HPLC/APCIMS) chromatograms of brGDGTs
 293 from (a) surface sediments from Gahai lake, and (b) soils in the catchment of Gahai lake.

294

295 *3.3 brGDGTs-temperature calibration and Holocene temperature reconstruction*

296 Gahai is a shallow lake in the eastern Tibetan Plateau that is typically completely frozen
 297 during winter and spring. Local meteorological data indicate that the average snowfall period
 298 lasts for 269 days, with around 50 days of continuous snowfall ([Luqu County Local](#)

299 [Chronicles Compilation Committee, 2006](#)). The freezing of the lake surface begins in late
300 October each year and gradually thaws starting from May of the following year. As a result,
301 the light transmittance and oxygen content in the lake water are reduced during the freezing
302 season, leading to decreased nutrient levels, which severely hinder the growth of autotrophic
303 microorganisms. Although the bacteria responsible for producing brGDGTs have not been
304 thoroughly characterized, the abundance of heterotrophic bacteria will likely decrease due to
305 the reduced autotrophic biomass during the winter and spring ice-covered period. The
306 weakened light penetration, decreased oxygen levels, and lack of nutrient replenishment
307 during the frozen period significantly impact the growth of autochthonous microorganisms.

308
309 ~~While the specific bacterial species responsible for brGDGT production are not yet well~~
310 ~~understood, it is known that these bacteria, as heterotrophic organisms, will also be~~
311 ~~influenced by the reduction in autotrophic biomass.~~ Furthermore, some research suggests that
312 the production of brGDGTs might be related to factors such as water depth, seasonal
313 alternation of water column mixing and stratification ([Loomis et al., 2014](#); [Van Bree et al.,](#)
314 [2020](#)). During the summer and autumn seasons when the lake ice melts and the water
315 becomes more mobile, the nutrient content increases, resulting in elevated lake biomass,
316 moreover, the oxygen levels at the bottom of Gahai lake are not expected to be too high,
317 which could further contribute to the proliferation of brGDGT-producing bacteria, potentially
318 leading to an increase in the brGDGT-producing bacteria ([Weber et al., 2018](#)). Therefore,
319 brGDGTs in Gahai lake may provide records of the average temperature during the ice-free
320 months of the summer and autumn seasons.

321
322 Additionally, the presence of the frozen lake surface during winter creates a thermal barrier,
323 impeding the exchange of heat between the lake water and the atmosphere. Consequently,
324 any brGDGTs generated within the lake water during this period lose their ability to
325 accurately reflect atmospheric temperature variations (Sun et al., 2021; Zhang et al., 2022a).
326 Thus, they were no longer able to track atmospheric temperature changes during the frozen
327 season. So, we prefer to use Gahai brGDGTs to reconstruct temperatures during the summer
328 and ice-free seasons. For this purpose, we employed the new Bayesian calibration for the
329 mean temperature of the Months Above Freezing (MAF), as proposed by Martínez-Sosa et al.
330 (2021), to derive a ~~warm-biased MAF temperature~~ for Gahai lake.

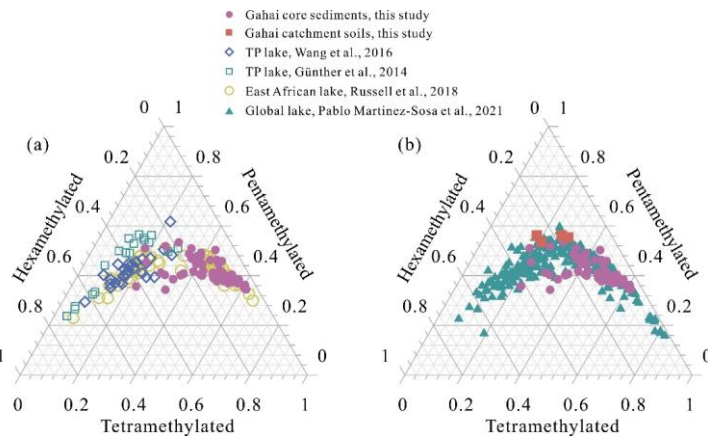
331
332 To assess the accuracy of this calibration approach, we compared the fractional abundances
333 of summed tetra-, penta-, and hexamethylated brGDGTs in Gahai lake sediments with other
334 datasets (Fig. 4). These datasets include lake sediments from the Tibetan Plateau (Günther et
335 al., 2014; Wang et al., 2016), East Africa (Russell et al., 2018), and global lakes (Martínez-
336 Sosa et al., 2021). The distribution pattern of Gahai core sediments is distinctly remarkable
337 compared to that of other lake sediments within the Tibetan Plateau, even though they share a
338 common regional origin (Fig. 4). However, its resemblance to the global distribution of
339 brGDGTs in lake sediments is evident. Notably, the calibration developed by Martínez-Sosa
340 et al. (2021) is based on brGDGTs from a global lake dataset.

341
342 Using calibration of Martínez-Sosa's et al. (2021), we reconstructed the surface sediment

343 temperature of Gahai lake, resulting in a temperature estimate of 9.4°C. This reconstructed
344 temperature closely matches the ice-free season temperature recorded by meteorological
345 stations in the Gahai region (8.8°C for May to September). Furthermore, considering the
346 significant contribution of autochthonous brGDGTs in Gahai lake, we also attempted to
347 reconstruct the Holocene paleotemperature record using previously published lake-specific
348 brGDGTs-temperature calibrations (e.g., ~~Dang et al., 2018~~; Günther et al., 2014; Martínez-
349 Sosa et al., 2021; Russell et al., 2018; Sun et al., 2011; Wang et al., 2016). As depicted in Fig.
350 S3, most of these calibrations exhibit qualitatively similar temperature change patterns when
351 applied to the sediment core from Gahai Lake. This similarity arises from their shared same
352 principles, just utilizing distinct datasets, resulting in records that display analogous trends
353 but vary in absolute temperatures. As illustrated in Fig. S3, most of these calibrations showed
354 qualitatively similar patterns of temperature change when applied to the sediment core from
355 Gahai lake. However, the magnitudes of temperature fluctuations varied considerably and
356 were found to be unsuitable for application in Gahai lake due to several key reasons. Firstly,
357 the fractional abundances of summed tetra-, penta-, and hexamethylated brGDGTs in Gahai
358 lake were inconsistent with those found in the reference datasets (Fig. 4). Secondly, the
359 analytical technique used for distinguishing 5- and 6-methyl isomers, which was a crucial
360 aspect of some calibration studies (Günther et al., 2014; Wang et al., 2016), was not
361 employed in those studies, resulting in their exclusion from our analysis. Thirdly, although
362 the brGDGTs fractions in Gahai lake are resembled those of East African lakes, the annual
363 mean temperature reconstructed using this calibration significantly differed from the
364 temperature data recorded at the Langmu Temple station. Moreover, even though the

365 ~~paleotemperature reconstruction for Gahai lake based on the warm season temperature~~
366 ~~calibration by Dang et al. (2018) showed similarity to the calibration by Martínez-Sosa et al.~~
367 ~~(2021). However, it is worth noting that the calibration by Dang et al. (2018) was established~~
368 ~~based on an investigation of 35 Chinese alkaline lakes, which may not be directly applicable~~
369 ~~to the freshwater environment of Gahai lake. Similarly, despite the salinity correction, the~~
370 ~~calibration reported by Wang et al. (2021) was not considered suitable for our study.~~

371



372

373 **Fig. 4** Comparison of the fractional abundances of tetramethylated, pentamethylated, and
374 hexamethylated bGDGTs in sediment core samples from Gahai with lake surface
375 sediments from the Tibetan Plateau (Wang et al., 2016; Günther et al., 2014), East Africa
376 (Russell et al., 2018), and worldwide (Martínez-Sosa et al., 2021).

377 ~~Given these limitations, we ultimately opted to use the new Bayesian calibration for the mean~~
378 ~~temperature of the Months Above Freezing, as proposed by Martínez-Sosa et al. (2021), to~~
379 ~~reconstruct a warm-biased temperature record for Gahai lake.~~

380

381 The depth interval of 191–279 cm in the Gahai sediment core represents an interval of rapid

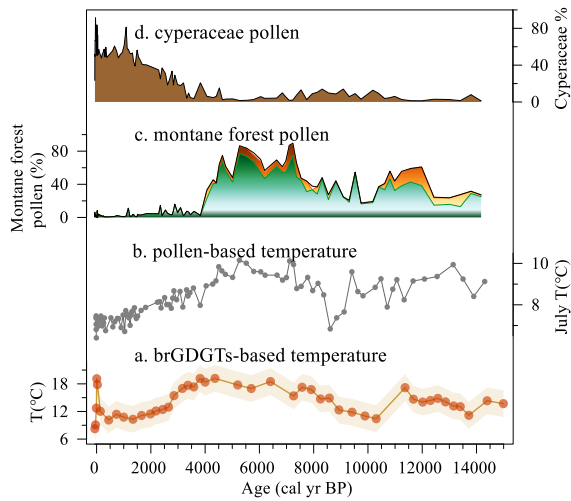
382 allocthonous sedimentation, or alternatively a slump, and therefore the results for the
383 corresponding time interval of 20–15 ka may be unreliable. Thus, our temperature record of
384 Months Above Freezing from the eastern TP spans the past 15 ka, with the average
385 temperature of 4°C, as shown in Fig. 5a. Within the range of age uncertainties, weak warming
386 occurred during 14.8–11.8 ka, likely to corresponding to the Bølling–Allerød (B/A)
387 interstadial. A minor cold reversal occurred during 11.8–10.5 ka, potentially corresponding to
388 the Younger Dryas (YD) event. Notably, the samples collected between 11.8 ka and 10.5 ka
389 exhibited GDGT concentrations below the detection limit. Therefore, we directly linked the
390 temperature reconstructions at the two aforementioned time points, ~11.8 ka and ~10.5 ka,
391 resulting in the lowest temperature of this time period appearing around 10.5 ka. This may
392 cause a time lag with the occurrence of the YD event. The temperature record indicates a
393 colder period during 11.5–8.0 ka. During 8.0–3.5 ka, Gahai experienced a stable warm period
394 with the average temperature of ~16.5°C, after which the temperature decreased gradually.
395 Overall, the maximum temperature difference since 15 ka was ~10°C. As for the absolute
396 temperature changes since 15,000 yr, although some influential studies indicate a warming of
397 approximately 6.1–7°C from the deglaciation onset to preindustrial times (Tierney et al., 2020;
398 Osman et al., 2021). However, these results are based on global mean sea surface
399 temperatures. Our reconstructed temperature range is about 10°C, considering the remarkable
400 ‘elevation-dependent warming’ observed in high-altitude regions compared to low-altitude
401 areas (Mountain Initiative EDW Working Group, 2015). Thus, this range could be accurate.
402 Nevertheless, we do not rule out the possibility that our temperature reconstruction may
403 exhibit an overestimation. ~~This is a known issue in temperature reconstruction using~~

404 ~~biomarkers~~—Aside from potential uncertainties associated with the biomarkers themselves,
405 calibrations may also considerably influence the observed amplitude. We examined
406 temperature variations reconstructed using different calibrations (Fig. S3), with the smallest
407 range being 6°C and the largest being 12°C. Undoubtedly, further efforts are needed to
408 constrain the inherent uncertainties related to biomarker-based temperature reconstructions.

409

410 *3.4 Holocene temperature changes on the eastern edge of TP and their origin*

411 Despite the difference in amplitude, the temperature record of Months Above Freezing from
412 Gahai resembles the pollen record and the pollen-based temperature reconstruction from the
413 same site (Fig. 5) (Wang et al., 2022). However, the brGDGTs-based Holocene Thermal
414 Maximum (HTM) lags the pollen-based reconstruction (Fig. 5a, b). Wang et al. (2022) used a
415 weighted-averaging partial least regression approach to produce a temperature record for
416 Gahai, based on a modern pollen dataset (n=731) from the eastern TP. Assessment of the
417 statistical significance of the pollen-based climate variables for Gahai suggests that the mean
418 July temperature is the most important environmental factor influencing the fossil pollen
419 assemblages. The brGDGTs in Gahai are indicative of summer and autumn temperatures, and
420 the mismatch between the temperature records inferred from brGDGTs and the pollen record
421 may be attributed to the difference between the solar irradiance during June–October and that
422 during July. A detailed analysis of this topic will be undertaken in the subsequent section.



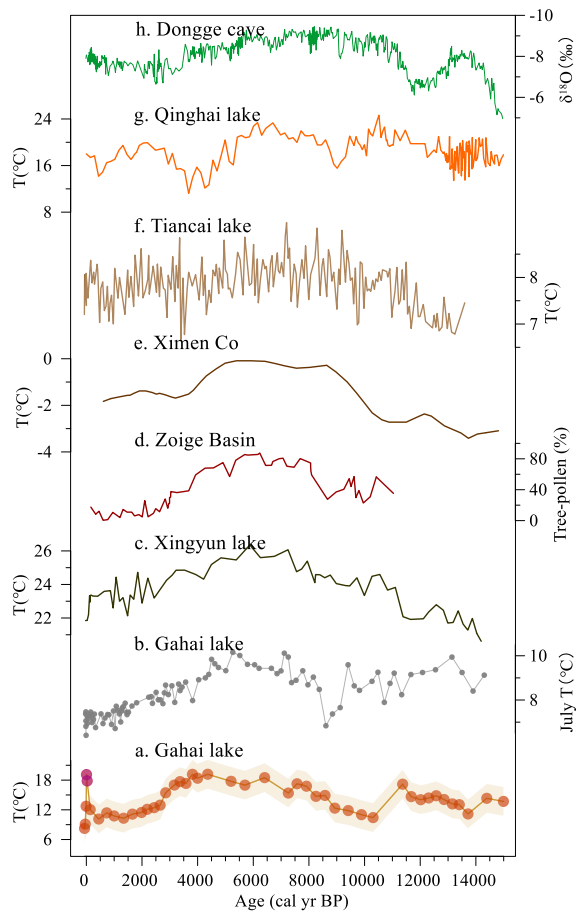
423

424 **Fig. 5** Comparison of multiproxy records from Gahai lake. (a) brGDGTs-based ~~warm-bias~~
 425 ~~temperature~~MAF (this study). (b) Temperature of the warmest month (July) based on
 426 pollen assemblages (Wang et al., 2022). (c, d) Pollen-reconstructed montane forest
 427 (*Pinus*, *Picea*, *Abies*) and Cyperaceae pollen record (Wang et al., 2022).

428

429 The brGDGTs-based temperature record from Gahai confirms the occurrence of a climate
 430 optimum in the mid-Holocene on the northeast Tibetan Plateau, which is consistent with
 431 several other pollen and pollen-reconstructed temperature records from the fringe areas of the
 432 Asian summer monsoon (Fig. 6), suggesting that it is a reliable representation of Holocene
 433 temperature changes in this region. For example, pollen-based temperature reconstructions
 434 from Xingyun lake and Ximen Co on the eastern TP show a early to middle HTM (9–4 ka)
 435 and a cooling trend thereafter (Fig. 6c, e) (Wu et al., 2018; Herzsuh et al., 2014; Wang et
 436 al., 2021a). Additionally, lake water temperature reconstructions based on subfossil
 437 chironomids from Tiancai lake (Fig. 6f) (Zhang et al., 2017; Zhang et al., 2019a) and

438 alkenones from Qinghai lake (Fig. 6g) (Hou et al., 2016) show the same trends during the
 439 past 15 ka, as also shown by other pollen-based temperature records from the TP (Chen et al.,
 440 2020). Pollen, chironomids and alkenones mainly respond to the growing season
 441 temperatures in middle and high latitudes, and thus the reconstructed temperature records are
 442 consistent with the variations in summer solar irradiance. Similar variations were documented
 443 in temperature reconstructions at a global scale (Marcott et al., 2013; Cartapanis et al., 2022).

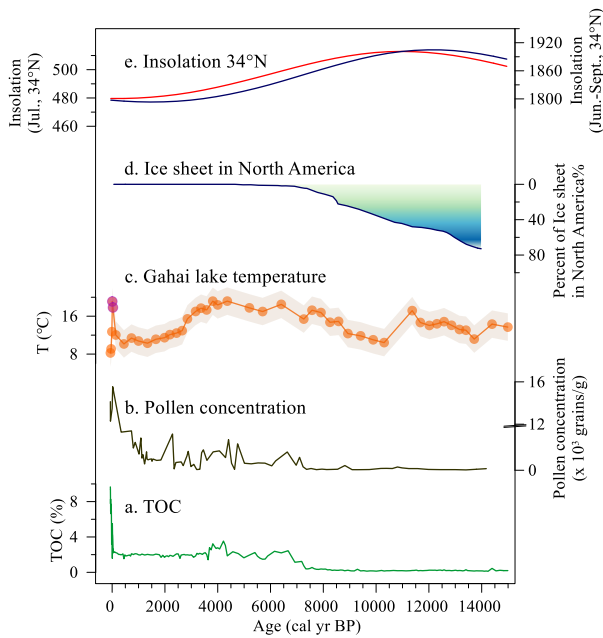


444
 445 **Fig. 6** Comparison of temperature at Gahai and other records from the eastern edge of the
 446 Tibetan Plateau. (a) brGDGTs-based ~~warm-bias temperature~~MAF at Gahai, the purple

447 dots may indicate unreliable temperature changes influenced by human activities (this
448 study). (b) Temperature of the warmest month (July) based on pollen data from Gahai
449 (Wang et al., 2022). (c) Pollen-based temperature at Xingyun lake (Wu et al., 2018). (d)
450 Tree pollen percentages from the Hongyuan peatland in the southern Zoige Basin (Zhou
451 et al., 2010). (e) Pollen-based temperature at Ximen Co (Herzschuh et al., 2014). (f)
452 Chironomid-based temperature at Tiancai lake (Zhang et al., 2017, 2019a). (g)
453 Alkenone-based temperature at Qinghai lake (Hou et al., 2016). (h) Stalagmite $\delta^{18}\text{O}$
454 record of Dongge cave (Dykoski et al., 2005).

455

456 Nevertheless, the timing and amplitude of the Gahai temperature fluctuations differ from
457 those of other temperature records from this region (Fig. 6). These discrepancies may be the
458 result of the chronological uncertainties of these records, and to differences in the seasonal
459 and spatial responses to climate forcing and feedbacks. The temperature records shown in Fig.
460 6 mostly refer to summer temperatures, which are primarily influenced by summer insolation.



461
 462 **Fig. 7** Temperature fluctuations and forcing factors during the Holocene. (a, b) TOC content
 463 and pollen concentrations from Gahai (Wang et al., 2022). (c) brGDGTs-based ~~warm-~~
 464 ~~bias-temperature~~MAF from Gahai, the purple dots may indicate unreliable temperature
 465 changes influenced by human activities (this study). (d) Percentage of the remnant
 466 Laurentide ice sheet in North America relative to the Last Glacial Maximum (Dyke,
 467 2004). (e) Local insolation at 34 °N during ice-free months (Laskar et al., 2004).

468
 469 The temperature record in Gahai during the early Holocene fails to closely track the Northern
 470 Hemisphere insolation trend, and there is also a time lag. The pollen-based temperature
 471 record for Xingyun Lake in southwestern China also shows lower temperatures in the early
 472 Holocene (Fig. 6c). The albedo effect caused by the increased cloud cover may be the reason
 473 for the early Holocene decrease in summer temperatures (Wu et al., 2018). However, the

474 pollen record from Gahai indicates dry conditions during the early Holocene (Wang et al.,
475 2022), and cloud cover may not be the primary factor responsible for the low temperatures at
476 this time. The melting of Northern Hemisphere ice sheets during the early Holocene
477 weakened the Atlantic Meridional Overturning Circulation (AMOC) and potentially also the
478 global thermohaline circulation. This led to a reduction in the amount of heat transport by the
479 North Atlantic warm current to high-latitude regions, which resulted in the low temperatures
480 in middle to high latitudes of the Northern Hemisphere. The persistence of the Laurentide ice
481 sheet into the early Holocene maintained the regional albedo, as well as discharging
482 meltwater into the North Atlantic (Fig. 7d) (Dyke, 2004). In addition, a Holocene temperature
483 simulation showed that global warming was more pronounced when dust factors were
484 excluded from the simulation (Liu et al. (2018). The record of insoluble particles in the
485 Greenland GISP2 ice core indicates relatively high concentrations of atmospheric aerosols in
486 the early Holocene (Zielinski and Mershon, 1997), which would have weakened summer
487 solar irradiation via radiative feedback, leading to the cool temperatures during this period.
488 These factors may together have caused the early Holocene temperature decline at Gahai
489 Lake, which slightly delayed the onset of the Holocene Warm Period.

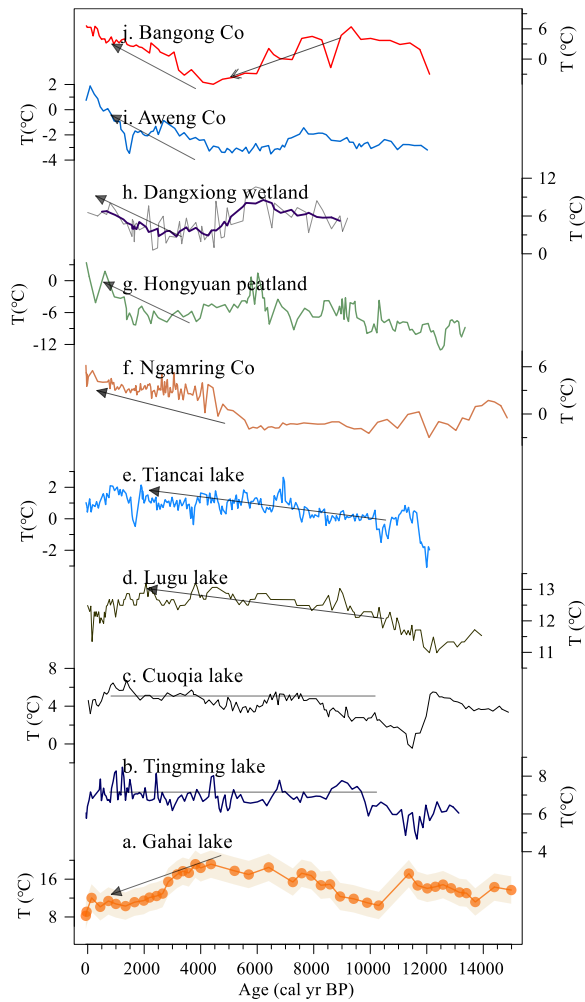
490
491 A notable and rapid temperature increase is evident at Gahai in recent decades, which differs
492 from the other records (Fig. 7c). Moreover, there are notable increases in pollen concentration,
493 TOC, and TN (Fig. 7a, b) in the Gahai sediment core, indicating intensive local human
494 activities like grazing and tourism, which may be the primary cause of the environmental
495 changes in this region (Wang et al., 2022). This intensive human activity may have reduced

496 the ability of the brGDGTs to record the natural temperature background. These observations
497 emphasize the important impact of human activities on climate proxies and the need to
498 carefully consider their effect on temperature reconstructions.

499

500 *3.5 Spatiotemporal pattern of brGDGTs-based TP temperatures*

501 In addition to comparing the Gahai temperature with the summer temperature records from
502 the eastern TP and its surrounding areas, we compiled and reviewed published Holocene
503 brGDGTs-based quantitative temperature records from across the TP. As shown in Fig. 8,
504 with the increasing number of these records for the TP, the differences between the results
505 have become more pronounced. The brGDGTs records from lakes in the central and western
506 parts of the plateau show higher temperatures in the early and late Holocene, and lower
507 temperatures in the middle Holocene (Wang et al., 2021c; Li et al., 2017; He et al., 2020),
508 while the brGDGTs records from lakes in the southern and south-eastern parts of the TP show
509 a warming trend throughout the Holocene (Sun et al., 2022; Feng et al., 2022). In addition,
510 brGDGTs in Cuoqia lake and Tingming lake, on the south-eastern TP, recorded the ice-free
511 season temperature, which was relatively stable during the Holocene (Sun et al., 2021; Zhang
512 et al., 2022a). However, our temperature record from Gahai is different from the above
513 records and resembles summer temperature changes during the Holocene (Chen et al., 2020).
514 This is because the brGDGTs record from Lake Gahai represents warm season temperatures,
515 which adds to its reliability.



516

517 **Fig. 8** Comparison of Holocene temperature based on brGDGTs at Gahai (a) and other
 518 records from around the TP. Reconstructed ice-free-season temperatures from (b)
 519 Tingming lake (Sun et al., 2021), (c) Cuoqia lake (Zhang et al., 2022a). Reconstructed
 520 annual temperature from (d) Lugu lake (Zhao et al., 2021b), (e) Tiancai lake (Feng et al.,
 521 2022), (f) Ngamring Co (Sun et al., 2022), (g) Hongyuan peatland (Yan et al., 2021). (h)
 522 Dangxiong wetland (Cheung et al., 2017), (i) Aweng Co (Li et al., 2017), (j) Bangong

523 Co (Wang et al., 2021c).

524

525 We suggest that the complexity of Holocene temperature patterns recorded by brGDGTs in
526 TP lakes is primarily due to the ambiguity of brGDGTs in these lakes, as well as to the spatial
527 heterogeneity of climate change across the TP. This ambiguity can be attributed to several
528 factors. First, the origin of brGDGTs in lakes remains an uncertain factor in temperature
529 reconstruction. An increasing number of studies indicate the occurrence of a remarkable
530 amount of autochthonous brGDGTs in lakes, but their abundance in soil can also affect the
531 distribution of brGDGTs in lakes due to their supply via soil erosion (e.g., Tierney and
532 Russell, 2009; Weber et al., 2015; Wang et al., 2023). In fact, even within the same lake (e.g.,
533 Tengchongqinghai lake in southwestern China), two studies reached inconsistent conclusions
534 regarding the origin of brGDGTs (Tian et al., 2019; Zhao et al., 2021b), possibly because the
535 niches of certain brGDGTs may expand or contract compared to other locations within a lake.
536 Therefore, it is important to conduct detailed modern process studies to accurately assess the
537 sources of brGDGTs in lakes, especially with regard to evaluating the proportion of
538 autochthonous brGDGTs (Wang et al., 2023; Martin et al., 2020). Second, brGDGTs may
539 show a seasonal signal. Current brGDGTs–temperature calibrations for lakes reflect the
540 annual average temperature (Sun et al., 2011; De Jonge et al., 2014), as well as the growing
541 season temperature (Sun et al., 2011; Dang et al., 2018) and the ice-free season temperature
542 (Martínez-Sosa et al., 2021; Zhang et al., 2022a). Thus, there is no consensus regarding
543 whether the brGDGTs have a seasonal bias, and it is necessary to conduct continuous, high-
544 resolution seasonal investigations of lakes on the Tibetan Plateau to comprehensively

545 elucidate the seasonal characteristics of brGDGTs. This can enhance the accuracy of regional
546 temperature reconstruction and may help reconcile the complex temperature patterns
547 observed on the Tibetan Plateau. Third, the factors affecting the distribution of brGDGTs in
548 lakes are complex, including not only temperature, pH and salinity but also oxygen content,
549 water depth, and so on (Wang et al., 2021b; Wang et al., 2016). The distribution of brGDGTs
550 in lakes is significantly influenced by the hydrological and physical properties of the lakes,
551 and thus it is necessary to attain a more comprehensive understanding of the characteristics of
552 the lakes in the study area and their effects on brGDGTs. Fourth, different brGDGTs–
553 temperature calibrations may lead to markable differences in both the amplitude and trend of
554 temperature from the same dataset (Wang et al., 2016; Feng et al., 2019). One reason for this
555 is the deviation between in-situ measured temperature and atmospheric temperature (Wang et
556 al., 2020). Thus, selecting an appropriate calibration and attempting to establish a brGDGTs–
557 in situ temperature calibration are effective means of enhancing the reliability of brGDGTs–
558 based temperature reconstructions.

559

560 **4 Conclusions**

561 We present a quantitative, brGDGTs-based seasonal paleotemperature record over the last 15
562 ka from the sediments of a shallow lake on the eastern Tibetan Plateau. Our reconstruction
563 resembles the summer temperature trend, with the Holocene Thermal Maximum occurring
564 during 8–3.5 ka. There is a lag between our brGDGTs-based reconstruction and pollen-based
565 July temperature recorded in the same sediment core, indicating a seasonal bias between
566 different proxies. Since 3.5 ka, the temperature decreased gradually, and the surficial

567 sediments reliably recorded the warm season temperature during the current period in the
568 Gahai Lake region. However, intensive local human activity during the last century has
569 affected the distribution of brGDGTs, resulting in temperature deviations recorded by
570 brGDGTs. However, the implementation of environmental protection policies have reduced
571 this anthropogenic signal. Our findings help better understand the seasonal signal of
572 brGDGTs in shallow lakes and provide important data for improving projections of terrestrial
573 climate change at high elevations.

574

575 We also investigated previously published brGDGTs-based Holocene temperature records on
576 the TP to determine the pattern of brGDGTs-based temperature changes and the possible
577 causes of the differences between reconstructions. We emphasize the need for the careful
578 examination of both the source and behavior of these compounds in lacustrine environments
579 and lake status, prior to the application of brGDGTs proxies in paleolimnological
580 reconstruction.

581

582 [Data availability](#)

583 [The data used in this study can be obtained from the corresponding author Juzhi Hou](#)
584 [\(houjz@itpcas.ac.cn\)](mailto:houjz@itpcas.ac.cn).

585

586 [Author contributions.](#)

587 [Xiaohuan Hou did the experiments, analyzed the data and wrote the manuscript. Nannan](#)
588 [Wang, Zhe Sun, Kan Yuan and Xianyong Cao participated in sample collecting and data](#)

589 analysis. Juzhi Hou designed this study and led the interpretation. All authors commented on
590 and improved the manuscript.

591

592 **Competing interests**

593 The contact author has declared that none of the authors has any competing interests.

594

595 **Acknowledgements**

596 This work was financially supported by the National Natural Science Foundation of China

597 (42025103, 41877459) and the Second Tibetan Plateau Scientific Expedition and Research

598 (2019QZKK0601). We would like to thank Jan Bloemendal for the help with language

599 editing.

600

References

- Bova, S., Rosenthal, Y., Liu, Z., Godad, S. P., and Yan, M.: Seasonal origin of the thermal maxima at the Holocene and the last interglacial, *Nature*, 589, 548-553, 10.1038/s41586-020-03155-x, 2021.
- Buckles, L. K., Weijers, J. W. H., Verschuren, D., and Damste, J. S. S.: Sources of core and intact branched tetraether membrane lipids in the lacustrine environment: Anatomy of Lake Challa and its catchment, equatorial East Africa, *Geochimica Et Cosmochimica Acta*, 140, 106-126, 10.1016/j.gca.2014.04.042, 2014.
- Cao, J., Rao, Z., Shi, F., and Jia, G.: Ice formation on lake surfaces in winter causes warm-season bias of lacustrine brGDGT temperature estimates, *Biogeosciences*, 17, 2521-2536, 10.5194/bg-17-2521-2020, 2020.
- Cartapanis, O., Jonkers, L., Moffa-Sanchez, P., Jaccard, S. L., and de Vernal, A.: Complex spatio-temporal structure of the Holocene Thermal Maximum, *Nat Commun*, 13, 5662, 10.1038/s41467-022-33362-1, 2022.
- Chen, D., Xu, B., Yao, T., Guo, Z., Cui, P., Chen, F., Zhang, R., Zhang, X., Zhang, Y., Fan, J., Hou, Z., and Zhang, T.: Assessment of past, present and future environmental changes on the Tibetan Plateau, *Chinese Science Bulletin*, 60, 3025-3035, 2015.
- Chen, F., Yu, Z., Yang, M., Ito, E., Wang, S., Madsen, D. B., Huang, X., Zhao, Y., Sato, T., Birks, H. J. B., Boomer, I., Chen, J., An, C., and Wünnemann, B.: Holocene moisture evolution in arid central Asia and its out-of-phase relationship with Asian monsoon history, *Quaternary Science Reviews*, 27, 351-364, 10.1016/j.quascirev.2007.10.017, 2008.
- Chen, F., Zhang, J., Liu, J., Cao, X., Hou, J., Zhu, L., Xu, X., Liu, X., Wang, M., Wu, D., Huang, L., Zeng, T., Zhang, S., Huang, W., Zhang, X., and Yang, K.: Climate change, vegetation history, and landscape responses on the Tibetan Plateau during the Holocene: A comprehensive review, *Quaternary Science Reviews*, 243, 10.1016/j.quascirev.2020.106444, 2020.
- Chen, Y., Zheng, F., Yang, H., Yang, W., Wu, R., Liu, X., Liang, H., Chen, H., Pei, H., Zhang, C., Pancost, R. D., and Zeng, Z.: The production of diverse brGDGTs by an Acidobacterium providing a physiological basis for paleoclimate proxies, *Geochimica et Cosmochimica Acta*, 337, 155-165, 10.1016/j.gca.2022.08.033, 2022.
- Cheung, M.-C., Zong, Y., Zheng, Z., Liu, Z., and Aitchison, J. C.: Holocene temperature and precipitation variability on the central Tibetan Plateau revealed by multiple palaeo-climatic proxy records from an alpine wetland sequence, *The Holocene*, 27, 1669-1681, 10.1177/0959683617702225, 2017.
- Committee, L. C. L. C. C.: Luqu County Chronicles, Gansu Cultural Publishing House, Lanzhou, 71 pp.2006.
- Crampton-Flood, E. D., Tierney, J. E., Peterse, F., Kirkels, F. M. S. A., and Damste, J. S. S.: BayMBT: A Bayesian calibration model for branched glycerol dialkyl glycerol tetraethers in soils and peats, *Geochimica Et Cosmochimica Acta*, 268, 142-159, 10.1016/j.gca.2019.09.043, 2020.
- Dang, X., Ding, W., Yang, H., Pancost, R. D., Naafs, B. D. A., Xue, J., Lin, X., Lu, J., and Xie, S.: Different temperature dependence of the bacterial brGDGT isomers in 35 Chinese lake sediments compared to that in soils, *Organic Geochemistry*, 119, 72-79,

设置了格式: 字体: 加粗

设置了格式: 字体: (默认) Times New Roman, 小四

645 10.1016/j.orggeochem.2018.02.008, 2018.
646 De Jonge, C., Hopmans, E. C., Zell, C. I., Kim, J.-H., Schouten, S., and Sinninghe Damsté, J.
647 S.: Occurrence and abundance of 6-methyl branched glycerol dialkyl glycerol tetraethers in
648 soils: Implications for palaeoclimate reconstruction, *Geochimica et Cosmochimica Acta*, 141,
649 97-112, 10.1016/j.gca.2014.06.013, 2014.
650 Ding, S., Xu, Y., Wang, Y., He, Y., Hou, J., Chen, L., and He, J. S.: Distribution of branched
651 glycerol dialkyl glycerol tetraethers in surface soils of the Qinghai-Tibetan Plateau:
652 implications of brGDGTs-based proxies in cold and dry regions, *Biogeosciences*, 12, 3141-
653 3151, 10.5194/bg-12-3141-2015, 2015.
654 Dong, Y., Wu, N., Li, F., Zhang, D., Zhang, Y., Shen, C., and Lu, H.: The Holocene
655 temperature conundrum answered by mollusk records from East Asia, *Nat Commun*, 13,
656 5153, 10.1038/s41467-022-32506-7, 2022.
657 Dyke, A. S.: An outline of North American deglaciation with emphasis on central and
658 northern Canada, *Quaternary Glaciations-Extent and Chronology, Pt 2: North America*, 2,
659 373-424, 10.1016/s1571-0866(04)80209-4, 2004.
660 Dykoski, C. A., Edwards, R. L., Cheng, H., Yuan, D. X., Cai, Y. J., Zhang, M. L., Lin, Y. S.,
661 Qing, J. M., An, Z. S., and Revenaugh, J.: A high-resolution, absolute-dated Holocene and
662 deglacial Asian monsoon record from Dongge Cave, China, *Earth and Planetary Science*
663 *Letters*, 233, 71-86, 10.1016/j.epsl.2005.01.036, 2005.
664 Feng, X., Zhao, C., D'Andrea, W. J., Liang, J., Zhou, A., and Shen, J.: Temperature
665 fluctuations during the Common Era in subtropical southwestern China inferred from
666 brGDGTs in a remote alpine lake, *Earth and Planetary Science Letters*, 510, 26-36,
667 10.1016/j.epsl.2018.12.028, 2019.
668 Feng, X., Zhao, C., D'Andrea, W. J., Hou, J., Yang, X., Xiao, X., Shen, J., Duan, Y., and Chen,
669 F.: Evidence for a Relatively Warm Mid - to Late Holocene on the Southeastern Tibetan
670 Plateau, *Geophysical Research Letters*, 49, 10.1029/2022gl098740, 2022.
671 Group, M. I. E. W.: Elevation-dependent warming in mountain regions of the world, *Nature*
672 *Climate Change*, 5, 424-430, 10.1038/nclimate2563, 2015.
673 Günther, F., Thiele, A., Gleixner, G., Xu, B., Yao, T., and Schouten, S.: Distribution of
674 bacterial and archaeal ether lipids in soils and surface sediments of Tibetan lakes:
675 Implications for GDGT-based proxies in saline high mountain lakes, *Organic Geochemistry*,
676 67, 19-30, 10.1016/j.orggeochem.2013.11.014, 2014.
677 Halamka, T. A., Raberg, J. H., McFarlin, J. M., Younkin, A. D., Mulligan, C., Liu, X. L., and
678 Kopf, S. H.: Production of diverse brGDGTs by *Acidobacterium Solibacter usitatus* in
679 response to temperature, pH, and O₂ provides a culturing perspective on brGDGT proxies
680 and biosynthesis, *Geobiology*, 10.1111/gbi.12525, 2022.
681 He, Y., Hou, J., Wang, M., Li, X., Liang, J., Xie, S., and Jin, Y.: Temperature Variation on the
682 Central Tibetan Plateau Revealed by Glycerol Dialkyl Glycerol Tetraethers From the
683 Sediment Record of Lake Linggo Co Since the Last Deglaciation, *Frontiers in Earth Science*,
684 8, 10.3389/feart.2020.574206, 2020.
685 Herzschuh, U., Borkowski, J., Schewe, J., Mischke, S., and Tian, F.: Moisture-advection
686 feedback supports strong early-to-mid Holocene monsoon climate on the eastern Tibetan
687 Plateau as inferred from a pollen-based reconstruction, *Palaeogeography, Palaeoclimatology,*
688 *Palaeoecology*, 402, 44-54, 10.1016/j.palaeo.2014.02.022, 2014.

689 Hou, J., Li, C., and Lee, S.: The temperature record of the Holocene: progress and
690 controversies, *Science Bulletin*, 10.1016/j.scib.2019.02.012, 2019.

691 Hou, J., Huang, Y., Zhao, J., Liu, Z., Colman, S., and An, Z.: Large Holocene summer
692 temperature oscillations and impact on the peopling of the northeastern Tibetan Plateau,
693 *Geophysical Research Letters*, 43, 1323-1330, 10.1002/2015gl067317, 2016.

694 Huguët, C., Hopmans, E. C., Febo-Ayala, W., Thompson, D. H., Sinninghe Damsté, J. S., and
695 Schouten, S.: An improved method to determine the absolute abundance of glycerol
696 dibiphytanyl glycerol tetraether lipids, *Organic Geochemistry*, 37, 1036-1041,
697 10.1016/j.orggeochem.2006.05.008, 2006.

698 Kuang, X. and Jiao, J. J.: Review on climate change on the Tibetan Plateau during the last
699 half century, *Journal of Geophysical Research: Atmospheres*, 121, 3979-4007,
700 10.1002/2015jd024728, 2016.

701 Laskar, J., Robutel, P., Joutel, F., Gastineau, M., Correia, A. C. M., and Levrard, B.: A long-
702 term numerical solution for the insolation quantities of the Earth, *Astronomy & Astrophysics*,
703 428, 261-285, 10.1051/0004-6361:20041335, 2004.

704 Li, X., Wang, M., Zhang, Y., Lei, L., and Hou, J.: Holocene climatic and environmental
705 change on the western Tibetan Plateau revealed by glycerol dialkyl glycerol tetraethers and
706 leaf wax deuterium-to-hydrogen ratios at Aweng Co, *Quaternary Research*, 87, 455-467,
707 10.1017/qua.2017.9, 2017.

708 Liu, Y., Zhang, M., Liu, Z., Xia, Y., Huang, Y., Peng, Y., and Zhu, J.: A Possible Role of Dust
709 in Resolving the Holocene Temperature Conundrum, *Scientific Reports*, 8, 10.1038/s41598-
710 018-22841-5, 2018.

711 Liu, Z. Y., Zhu, J., Rosenthal, Y., Zhang, X., Otto-Bliesner, B. L., Timmermann, A., Smith, R.
712 S., Lohmann, G., Zheng, W. P., and Timm, O. E.: The Holocene temperature conundrum,
713 *Proc. Natl. Acad. Sci. U. S. A.*, 111, E3501-E3505, 10.1073/pnas.1407229111, 2014.

714 Loomis, S. E., Russell, J. M., Heuereux, A. M., D'Andrea, W. J., and Sinninghe Damsté, J. S.:
715 Seasonal variability of branched glycerol dialkyl glycerol tetraethers (brGDGTs) in a
716 temperate lake system, *Geochimica et Cosmochimica Acta*, 144, 173-187,
717 10.1016/j.gca.2014.08.027, 2014.

718 Lu, H., Wu, N., Liu, K.-b., Zhu, L., Yang, X., Yao, T., Wang, L., Li, Q., Liu, X., Shen, C., Li,
719 X., Tong, G., and Jiang, H.: Modern pollen distributions in Qinghai-Tibetan Plateau and the
720 development of transfer functions for reconstructing Holocene environmental changes,
721 *Quaternary Science Reviews*, 30, 947-966, 10.1016/j.quascirev.2011.01.008, 2011.

722 Ma, W., Li, G., Song, J., Yan, L., and Wu, L.: Effect of Vegetation Degradation on Soil
723 Organic Carbon Pool and Carbon Pool Management Index in the Gahai Wetland, China, *Acta*
724 *Agrestia Sinica*, 27, 687-694, 2019.

725 Marcott, S. A., Shakun, J. D., Clark, P. U., and Mix, A. C.: A Reconstruction of Regional and
726 Global Temperature for the Past 11,300 Years, *Science*, 339, 1198-1201,
727 10.1126/science.1228026, 2013.

728 Marsicek, J., Shuman, B. N., Bartlein, P. J., Shafer, S. L., and Brewer, S.: Reconciling
729 divergent trends and millennial variations in Holocene temperatures, *Nature*, 554, 92-+,
730 10.1038/nature25464, 2018.

731 Martin, C., Ménot, G., Thouveny, N., Peyron, O., Andrieu-Ponel, V., Montade, V., Davtian,
732 N., Reille, M., and Bard, E.: Early Holocene Thermal Maximum recorded by branched

733 tetraethers and pollen in Western Europe (Massif Central, France), *Quaternary Science*
734 *Reviews*, 228, 106109, 10.1016/j.quascirev.2019.106109, 2020.

735 Martínez-Sosa, P., Tierney, J. E., Stefanescu, I. C., Dearing Crampton-Flood, E., Shuman, B.
736 N., and Routson, C.: A global Bayesian temperature calibration for lacustrine brGDGTs,
737 *Geochimica et Cosmochimica Acta*, 305, 87-105, 10.1016/j.gca.2021.04.038, 2021.

738 Moser, K. A., Baron, J. S., Brahney, J., Oleksy, I. A., Saros, J. E., Hundey, E. J., Sadro, S.,
739 Kopáček, J., Sommaruga, R., Kainz, M. J., Strecker, A. L., Chandra, S., Walters, D. M.,
740 Preston, D. L., Michelutti, N., Lepori, F., Spaulding, S. A., Christianson, K. R., Melack, J. M.,
741 and Smol, J. P.: Mountain lakes: Eyes on global environmental change, *Global and Planetary*
742 *Change*, 178, 77-95, 10.1016/j.gloplacha.2019.04.001, 2019.

743 Opitz, S., Zhang, C., Herzschuh, U., and Mischke, S.: Climate variability on the south-eastern
744 Tibetan Plateau since the Lateglacial based on a multiproxy approach from Lake Naleng –
745 comparing pollen and non-pollen signals, *Quaternary Science Reviews*, 115, 112-122,
746 10.1016/j.quascirev.2015.03.011, 2015.

747 Osman, M. B., Tierney, J. E., Zhu, J., Tardif, R., Hakim, G. J., King, J., and Poulsen, C. J.:
748 Globally resolved surface temperatures since the Last Glacial Maximum, *Nature*, 599, 239-
749 244, 10.1038/s41586-021-03984-4, 2021.

750 Pang, H., Hou, S., Zhang, W., Wu, S., Jenk, T. M., Schwikowski, M., and Jouzel, J.:
751 Temperature Trends in the Northwestern Tibetan Plateau Constrained by Ice Core Water
752 Isotopes Over the Past 7,000 Years, *Journal of Geophysical Research-Atmospheres*, 125,
753 10.1029/2020jd032560, 2020.

754 Qiu, J.: The third pole, *Nature*, 454, 393-396, 10.1038/454393a, 2008.

755 Russell, J. M., Hopmans, E. C., Loomis, S. E., Liang, J., and Sinninghe Damsté, J. S.:
756 Distributions of 5- and 6-methyl branched glycerol dialkyl glycerol tetraethers (brGDGTs) in
757 East African lake sediment: Effects of temperature, pH, and new lacustrine paleotemperature
758 calibrations, *Organic Geochemistry*, 117, 56-69, 10.1016/j.orggeochem.2017.12.003, 2018.

759 Sinninghe Damsté, J. S., Hopmans, E. C., Pancost, R. D., Schouten, S., and Geenevasen, J. A.
760 J.: Newly discovered non-isoprenoid glycerol dialkyl glycerol tetraether lipids in sediments,
761 *Chemical Communications*, 1683-1684, 10.1039/b004517i, 2000.

762 Sinninghe Damsté, J. S., Ossebaar, J., Abbas, B., Schouten, S., and Verschuren, D.: Fluxes
763 and distribution of tetraether lipids in an equatorial African lake: Constraints on the
764 application of the TEX86 palaeothermometer and BIT index in lacustrine settings,
765 *Geochimica et Cosmochimica Acta*, 73, 4232-4249, 10.1016/j.gca.2009.04.022, 2009.

766 Sun, Q., Chu, G., Liu, M., Xie, M., Li, S., Ling, Y., Wang, X., Shi, L., Jia, G., and Lü, H.:
767 Distributions and temperature dependence of branched glycerol dialkyl glycerol tetraethers in
768 recent lacustrine sediments from China and Nepal, *Journal of Geophysical Research*, 116,
769 10.1029/2010jg001365, 2011.

770 Sun, X., Zhao, C., Zhang, C., Feng, X., Yan, T., Yang, X., and Shen, J.: Seasonality in
771 Holocene Temperature Reconstructions in Southwestern China, *Paleoceanography and*
772 *Paleoclimatology*, 36, 10.1029/2020pa004025, 2021.

773 Sun, Z., Hou, X., Ji, K., Yuan, K., Li, C., Wang, M., and Hou, J.: Potential winter-season bias
774 of annual temperature variations in monsoonal Tibetan Plateau since the last deglaciation,
775 *Quaternary Science Reviews*, 292, 10.1016/j.quascirev.2022.107690, 2022.

776 Thompson, L. G., Yao, T., Davis, M. E., Henderson, K. A., MosleyThompson, E., Lin, P. N.,

777 Beer, J., Synal, H. A., ColeDai, J., and Bolzan, J. F.: Tropical climate instability: The last
778 glacial cycle from a Qinghai-Tibetan ice core, *Science*, 276, 1821-1825,
779 10.1126/science.276.5320.1821, 1997.

780 Tian, L., Wang, M., Zhang, X., Yang, X., Zong, Y., Jia, G., Zheng, Z., and Man, M.:
781 Synchronous change of temperature and moisture over the past 50 ka in subtropical
782 southwest China as indicated by biomarker records in a crater lake, *Quaternary Science*
783 *Reviews*, 212, 121-134, 10.1016/j.quascirev.2019.04.003, 2019.

784 Tierney, J. E. and Russell, J. M.: Distributions of branched GDGTs in a tropical lake system:
785 Implications for lacustrine application of the MBT/CBT paleoproxy, *Organic Geochemistry*,
786 40, 1032-1036, 10.1016/j.orggeochem.2009.04.014, 2009.

787 Tierney, J. E., Russell, J. M., Eggermont, H., Hopmans, E. C., Verschuren, D., and Sinninghe
788 Damsté, J. S.: Environmental controls on branched tetraether lipid distributions in tropical
789 East African lake sediments, *Geochimica et Cosmochimica Acta*, 74, 4902-4918,
790 10.1016/j.gca.2010.06.002, 2010.

791 Tierney, J. E., Zhu, J., King, J., Malevich, S. B., Hakim, G. J., and Poulsen, C. J.: Glacial
792 cooling and climate sensitivity revisited, *Nature*, 584, 569-+, 10.1038/s41586-020-2617-x,
793 2020.

794 van Bree, L. G. J., Peterse, F., Baxter, A. J., De Crop, W., van Grinsven, S., Villanueva, L.,
795 Verschuren, D., and Sinninghe Damsté, J. S.: Seasonal variability and sources of in situ
796 brGDGT production in a permanently stratified African crater lake, *Biogeosciences*, 17,
797 5443-5463, 10.5194/bg-17-5443-2020, 2020.

798 Wang, G., Wang, Y., Wei, Z., He, W., Ma, X., and Zhang, T.: Reconstruction of temperature
799 and precipitation spanning the past 28 kyr based on branched tetraether lipids from Qionghai
800 Lake, southwestern China, *Palaeogeography Palaeoclimatology Palaeoecology*, 562,
801 10.1016/j.palaeo.2020.110094, 2021a.

802 Wang, H., An, Z., Lu, H., Zhao, Z., and Liu, W.: Calibrating bacterial tetraether distributions
803 towards in situ soil temperature and application to a loess-paleosol sequence, *Quaternary*
804 *Science Reviews*, 231, 10.1016/j.quascirev.2020.106172, 2020.

805 Wang, H., Chen, W., Zhao, H., Cao, Y., Hu, J., Zhao, Z., Cai, Z., Wu, S., Liu, Z., and Liu, W.:
806 Biomarker-based quantitative constraints on maximal soil-derived brGDGTs in modern lake
807 sediments, *Earth and Planetary Science Letters*, 602, 10.1016/j.epsl.2022.117947, 2023.

808 Wang, H., Liu, W., He, Y., Zhou, A., Zhao, H., Liu, H., Cao, Y., Hu, J., Meng, B., Jiang, J.,
809 Kolpakova, M., Krivonogov, S., and Liu, Z.: Salinity-controlled isomerization of lacustrine
810 brGDGTs impacts the associated MBT5ME' terrestrial temperature index, *Geochimica et*
811 *Cosmochimica Acta*, 305, 33-48, 10.1016/j.gca.2021.05.004, 2021b.

812 Wang, M., Liang, J., Hou, J., and Hu, L.: Distribution of GDGTs in lake surface sediments on
813 the Tibetan Plateau and its influencing factors, *Science China Earth Sciences*, 59, 961-974,
814 10.1007/s11430-015-5214-3, 2016.

815 Wang, M. D., Hou, J. Z., Duan, Y. W., Chen, J. H., Li, X. M., He, Y., Lee, S. Y., and Chen, F.
816 H.: Internal feedbacks forced Middle Holocene cooling on the Qinghai-Tibetan Plateau,
817 *Boreas*, 10.1111/bor.12531, 2021c.

818 Wang, N., Liu, L., Hou, X., Zhang, Y., Wei, H., and Cao, X.: Palynological evidence reveals
819 an arid early Holocene for the northeast Tibetan Plateau, *Climate of the Past*, 18, 2381-2399,
820 10.5194/cp-18-2381-2022, 2022.

821 Weber, Y., De Jonge, C., Rijpstra, W. I. C., Hopmans, E. C., Stadnitskaia, A., Schubert, C. J.,
822 Lehmann, M. F., Sinninghe Damsté, J. S., and Niemann, H.: Identification and carbon isotope
823 composition of a novel branched GDGT isomer in lake sediments: Evidence for lacustrine
824 branched GDGT production, *Geochimica et Cosmochimica Acta*, 154, 118-129,
825 10.1016/j.gca.2015.01.032, 2015.

826 Weber, Y., Sinninghe Damsté, J. S., Zopfi, J., De Jonge, C., Gilli, A., Schubert, C. J., Lepori,
827 F., Lehmann, M. F., and Niemann, H.: Redox-dependent niche differentiation provides
828 evidence for multiple bacterial sources of glycerol tetraether lipids in lakes, *Proc Natl Acad*
829 *Sci U S A*, 115, 10926-10931, 10.1073/pnas.1805186115, 2018.

830 Weijers, J. W. H., Schouten, S., van den Donker, J. C., Hopmans, E. C., and Sinninghe
831 Damsté, J. S.: Environmental controls on bacterial tetraether membrane lipid distribution in
832 soils, *Geochimica et Cosmochimica Acta*, 71, 703-713, 10.1016/j.gca.2006.10.003, 2007.

833 Woltering, M., Werne, J. P., Kish, J. L., Hicks, R., Sinninghe Damsté, J. S., and Schouten, S.:
834 Vertical and temporal variability in concentration and distribution of thaumarchaeotal
835 tetraether lipids in Lake Superior and the implications for the application of the TEX86
836 temperature proxy, *Geochimica et Cosmochimica Acta*, 87, 136-153,
837 10.1016/j.gca.2012.03.024, 2012.

838 Wu, D., Chen, X., Lv, F., Brenner, M., Curtis, J., Zhou, A., Chen, J., Abbott, M., Yu, J., and
839 Chen, F.: Decoupled early Holocene summer temperature and monsoon precipitation in
840 southwest China, *Quaternary Science Reviews*, 193, 54-67, 10.1016/j.quascirev.2018.05.038,
841 2018.

842 Wu, J., Yang, H., Pancost, R. D., Naafs, B. D. A., Qian, S., Dang, X., Sun, H., Pei, H., Wang,
843 R., Zhao, S., and Xie, S.: Variations in dissolved O₂ in a Chinese lake drive changes in
844 microbial communities and impact sedimentary GDGT distributions, *Chemical Geology*, 579,
845 10.1016/j.chemgeo.2021.120348, 2021.

846 Yan, T., Zhao, C., Yan, H., Shi, G., Sun, X., Zhang, C., Feng, X., and Leng, C.: Elevational
847 differences in Holocene thermal maximum revealed by quantitative temperature
848 reconstructions at ~30° N on eastern Tibetan Plateau, *Palaeogeography, Palaeoclimatology,*
849 *Palaeoecology*, 570, 110364, 10.1016/j.palaeo.2021.110364, 2021.

850 Yao, T., Bolch, T., Chen, D., Gao, J., Immerzeel, W., Piao, S., Su, F., Thompson, L., Wada, Y.,
851 Wang, L., Wang, T., Wu, G., Xu, B., Yang, W., Zhang, G., and Zhao, P.: The imbalance of the
852 Asian water tower, *Nature Reviews Earth & Environment*, 3, 618-632, 10.1038/s43017-022-
853 00299-4, 2022.

854 Zhang, C., Zhao, C., Yu, S.-Y., Yang, X., Cheng, J., Zhang, X., Xue, B., Shen, J., and Chen, F.:
855 Seasonal imprint of Holocene temperature reconstruction on the Tibetan Plateau, *Earth-*
856 *Science Reviews*, 226, 103927, 10.1016/j.earscirev.2022.103927, 2022a.

857 Zhang, E., Chang, J., Shulmeister, J., Langdon, P., Sun, W., Cao, Y., Yang, X., and Shen, J.:
858 Summer temperature fluctuations in Southwestern China during the end of the LGM and the
859 last deglaciation, *Earth and Planetary Science Letters*, 509, 78-87, 10.1016/j.epsl.2018.12.024,
860 2019a.

861 Zhang, E., Chang, J., Cao, Y., Sun, W., Shulmeister, J., Tang, H., Langdon, P. G., Yang, X.,
862 and Shen, J.: Holocene high-resolution quantitative summer temperature reconstruction based
863 on subfossil chironomids from the southeast margin of the Qinghai-Tibetan Plateau,
864 *Quaternary Science Reviews*, 165, 1-12, 10.1016/j.quascirev.2017.04.008, 2017.

865 Zhang, G., Luo, W., Chen, W., and Zheng, G.: A robust but variable lake expansion on the
866 Tibetan Plateau, *Science Bulletin*, 64, 1306-1309, 10.1016/j.scib.2019.07.018, 2019b.
867 Zhang, W., Wu, H., Cheng, J., Geng, J., Li, Q., Sun, Y., Yu, Y., Lu, H., and Guo, Z.: Holocene
868 seasonal temperature evolution and spatial variability over the Northern Hemisphere
869 landmass, *Nat Commun*, 13, 5334, 10.1038/s41467-022-33107-0, 2022b.
870 Zhao, B., Castaneda, I. S., Bradley, R. S., Salacup, J. M., de Wet, G. A., Daniels, W. C., and
871 Schneider, T.: Development of an in situ branched GDGT calibration in Lake 578, southern
872 Greenland, *Organic Geochemistry*, 152, 10.1016/j.orggeochem.2020.104168, 2021a.
873 Zhao, C., Liu, Z. H., Rohling, E. J., Yu, Z. C., Liu, W. G., He, Y. X., Zhao, Y., and Chen, F. H.:
874 Holocene temperature fluctuations in the northern Tibetan Plateau, *Quaternary Research*, 80,
875 55-65, 10.1016/j.yqres.2013.05.001, 2013.
876 Zhao, C., Rohling, E. J., Liu, Z., Yang, X., Zhang, E., Cheng, J., Liu, Z., An, Z., Yang, X.,
877 Feng, X., Sun, X., Zhang, C., Yan, T., Long, H., Yan, H., Yu, Z., Liu, W., Yu, S.-Y., and Shen,
878 J.: Possible obliquity-forced warmth in southern Asia during the last glacial stage, *Science*
879 *Bulletin*, 66, 1136-1145, 10.1016/j.scib.2020.11.016, 2021b.
880 Zheng, Y., Li, Q., Wang, Z., Naafs, B. D. A., Yu, X., and Pancost, R. D.: Peatland GDGT
881 records of Holocene climatic and biogeochemical responses to the Asian Monsoon, *Organic*
882 *Geochemistry*, 87, 86-95, 10.1016/j.orggeochem.2015.07.012, 2015.
883 Zhou, W., Yu, S.-Y., Burr, G. S., Kukla, G. J., Jull, A. J. T., Xian, F., Xiao, J., Colman, S. M.,
884 Yu, H., Liu, Z., and Kong, X.: Postglacial changes in the Asian summer monsoon system: a
885 pollen record from the eastern margin of the Tibetan Plateau, *Boreas*, 39, 528-539,
886 10.1111/j.1502-3885.2010.00150.x, 2010.
887 Zielinski, G. A. and Mershon, G. R.: Paleoenviromental implications of the insoluble
888 microparticle record in the GISP2 (Greenland) ice core during the rapidly changing climate
889 of the Pleistocene-Holocene transition, *Geological Society of America Bulletin*, 109, 547-559,
890 10.1130/0016-7606(1997)109<0547:piotim>2.3.co;2, 1997.

891

892